



Enhanced plasticity of FeCoBSiNb bulk glassy alloys by controlling the structure heterogeneity with Cu addition

Long Hou^a, Qianqian Wang^a, Weiming Yang^b, Baolong Shen^{a,b,*}

^a School of Materials Science and Engineering, Jiangsu Key Laboratory for Advanced Metallic Materials, Southeast University, Nanjing 211189, China

^b Institute of Massive Amorphous Metal Science, China University of Mining and Technology, Xuzhou 221116, China



ARTICLE INFO

Keywords:

Fe-based bulk glassy alloys
Cu addition
Large plasticity
High strength
Soft magnetic properties
Heterogeneous structure

ABSTRACT

In this work, an FeCoBSiNbCu bulk glassy alloy (BGA) with a diameter up to 4 mm was successfully prepared by copper mold casting method. The $(\text{Fe}_{0.5}\text{Co}_{0.5})_{71.6}\text{B}_{20}\text{Si}_4\text{Nb}_4\text{Cu}_{0.4}$ BGA exhibits a high strength over 4 GPa and an enhanced plasticity of 3.7%, combined with good soft magnetic properties. A well-developed vein pattern on the fracture surface and highly dense multiple shear bands throughout the overall rod were observed on the deformed specimen. The improved plasticity is strongly related to the nano-scale heterogeneous structure introduced to the glassy alloy by phase separation with minor Cu addition, which can hinder the propagation of shear bands, promote multiple shearing and enhance the plasticity. This work might have a guiding significance for a deep-understanding of the plastic deformation mechanism of Fe-based BGA in a high strength level.

1. Introduction

Since the first ferromagnetic bulk glassy alloy (BGA) FeAlGaPCB was formed in 1995 [1], a variety of Fe-based BGAs have been synthesized [2–7]. Especially, after the FeCoBSiNb and FeMoPCBSi BGAs with excellent soft magnetic properties and good glass-forming ability (GFA) were successfully prepared [8,9], they were considered to possess promising applications as magnetic, structural and surface coating materials. However, most of the Fe-based BGAs are prone to catastrophic brittle failure when deformed at room temperature, which limits their large-scale applications. Thus, it is important from a commercial perspective to enhance the plasticity of Fe-based BGAs at room temperature. Recently, a novel ductile CoFeBSiNb BGA with minor Cu addition, exhibiting an enhanced compressive plastic strain of 2.5% and extremely high fracture strength of 4.4 GPa was reported [10]. It was found that the addition of Cu induces a large number of α -(Fe,Co) nanoparticles disperse in the glassy matrix, which promote the generation of multiple shear bands and prevent the sudden brittle fracture of Co-FeBSiNb rod samples. Meanwhile, a novel ductile FeBSiPNb BGA with partial substitution of Fe by Ni exhibited an obviously enhanced plastic strain of 7.8%, but a lower fracture strength of 3.35 GPa [11], resulted from the unique atomic configuration containing both non-directional metal-metal bonds and directional metal-metalloid bonds. As both high fracture strength and good plastic deformation ability are imperative

for structural applications of Fe-based BGAs, it is worth exploring a Fe-based BGA with not only high strength but also satisfying plasticity. Among all of the Fe-based BGA system, FeCoBSiNb BGA possesses a large GFA and excellent soft magnetic properties, as well as high strength [8]. However, their low plasticity restricts their further applications. Although some researchers have tried to elucidate the influence of minor Cu addition on the plastic deformation behavior of FeCoBSiNb BGA [12], the improvement of plasticity from the phase separation by adding Cu has not been fully investigated. Moreover, the phase separation in the amorphous matrix has obvious impact on the soft magnetic properties of glassy alloys [13,14]. The multiple effect of phase separation in FeCoBSiNbCu BGA on their soft magnetic properties and plastic strain hasn't been studied.

In this work, to improve the plasticity of Fe-based BGA without obvious reduction in strength or soft magnetic properties, minor addition of Cu in FeCoBSiNb glassy system to induce the heterogeneous structure was studied. As a result, $(\text{Fe}_{0.5}\text{Co}_{0.5})_{72-x}\text{B}_{20}\text{Si}_4\text{Nb}_4\text{Cu}_x$ ($x = 0, 0.3, 0.4, 0.7$ and 1 at.%) BGAs with large GFA, high fracture strength and high plastic strain were successfully prepared. The thermal stability, deformation behaviors at room temperature, as well as soft magnetic properties of these Fe-based BGAs were investigated in detail.

* Corresponding author at: School of Materials Science and Engineering, Jiangsu Key Laboratory for Advanced Metallic Materials, Southeast University, Nanjing 211189, China.

E-mail address: blshen@seu.edu.cn (B. Shen).

<https://doi.org/10.1016/j.jnoncrysol.2018.11.015>

Received 18 September 2018; Received in revised form 11 November 2018; Accepted 14 November 2018

Available online 23 November 2018

0022-3093/ © 2018 Elsevier B.V. All rights reserved.

2. Experimental

2.1. Preparation of Fe-based alloys

Multi-component alloy ingots with nominal compositions of $(\text{Fe}_{0.5}\text{Co}_{0.5})_{72-x}\text{B}_{20}\text{Si}_4\text{Nb}_4\text{Cu}_x$ ($x = 0, 0.3, 0.4, 0.7$ and 1 at.%) were prepared by arc melting the mixtures of pure Fe (99.99 wt%), Cu (99.995 wt%), Co (99.99 wt%), Nb (99.95 wt%), B (99.99 wt%) and Si (99.999 wt%) in a highly purified argon atmosphere. The ribbons with a width of 2 mm and a thickness of 28 μm were produced by single-roller melt spinning method, and the cylindrical glassy rods with diameters up to 4 mm were prepared by copper-mold casting method.

2.2. Characterization and tests

The glassy structure of samples was characterized by X-ray diffraction (XRD, Bruker D8 Discover) with $\text{Cu K}\alpha$ radiation and transmission electron microscopy (TEM, JEM2000ex). The free side of ribbon and powder of crushed rod samples were used for XRD detection, respectively. The thermal stability was examined using a differential scanning calorimeter (DSC, NETZSCH 404 F3) under a flow of high purity argon with a heating rate of 0.67 K/s. The saturation magnetization (B_s) and coercivity (H_c) were measured with a vibrating sample magnetometer (VSM, Lake Shore 7410) under an applied field of 800 kA/m, and a B - H loop tracer (RIKEN BHS-40) under a field of 1 kA/m, respectively. The uniaxial compression test was performed on the testing machine (CMT 4503) at room temperature. The specimens used in the compression tests were prepared in the form of cylinder with a diameter of 1 mm and a length of 2 mm. Both top and bottom faces were polished carefully to ensure parallelism. Before compression tests, the sample was put in the center of the down-pressure plate vertically. The distance between up-pressure plate and top of the sample was adjusted to prevent tilting during the initial pressing process. The initial displacement from this step was cleared in related computer software (Powertest 4.0). The compression rate of the tests was set to 0.06 mm/min (strain rate: $5 \times 10^{-4} \text{ s}^{-1}$). The morphology of the deformation and fracture surfaces were examined by scanning electron microscopy (SEM, FEI Sirion 200). Measurement errors for thermal parameters were determined by analyzing the values of five measurements, and for magnetic H_c , plastic strain ϵ_p and strain-hardening exponent n were determined by averaging the measured values of three specimens.

3. Results and discussion

All of the melt-spun ribbons used for thermal and magnetic tests are composed of a fully glassy phase without any crystallization confirmed by their XRD, TEM and selected area electron diffraction (SAED) patterns (data not shown here). Fig. 1 shows the heating DSC curves of melt-spun $(\text{Fe}_{0.5}\text{Co}_{0.5})_{72-x}\text{B}_{20}\text{Si}_4\text{Nb}_4\text{Cu}_x$ ($x = 0, 0.3, 0.4, 0.7$ and 1 at.%) glassy ribbons. As shown in the figure, all of the glassy alloys undergo glass transition events, followed by a supercooled liquid region and then crystallization, but the glass transition becomes weak gradually as Cu content increases from 0.3 to 1 at.%. In addition, it is interesting to see that the crystallization behavior changes from two-stage to single stage as Cu content increases from 0 to 0.3 at.%, but changes to two-stage again as the Cu content increases to 0.4 at.%, then even changes to three-stage with further increase of Cu content to 0.7 and 1 at.%, as three exothermic peaks can be clearly seen in the DSC curves indexed as P_1 , P_2 and P_3 in the figure. To further investigate the effect of Cu addition on the thermal stability of FeCoBSiNb amorphous alloys, the crystallization behavior of $(\text{Fe}_{0.5}\text{Co}_{0.5})_{72-x}\text{B}_{20}\text{Si}_4\text{Nb}_4\text{Cu}_x$ ($x = 0$ and 1 at.%) were thoroughly studied by annealing the samples at different temperatures. Fig. 2 (a) shows the XRD patterns of $(\text{Fe}_{0.5}\text{Co}_{0.5})_{72}\text{B}_{20}\text{Si}_4\text{Nb}_4$ glassy ribbons annealed at 828 K and 900 K, corresponding to the temperatures just below and above the first

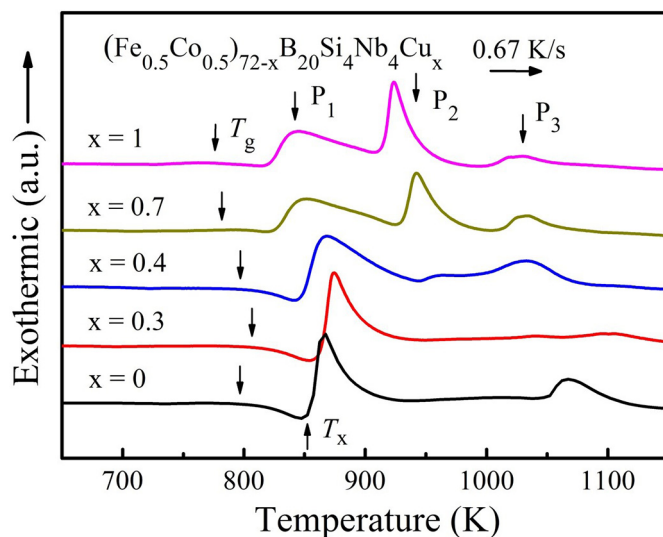


Fig. 1. DSC curves of $(\text{Fe}_{0.5}\text{Co}_{0.5})_{72-x}\text{B}_{20}\text{Si}_4\text{Nb}_4\text{Cu}_x$ ($x = 0, 0.3, 0.4, 0.7$ and 1 at.%) glassy ribbons with a heating rate of 0.67 K/s.

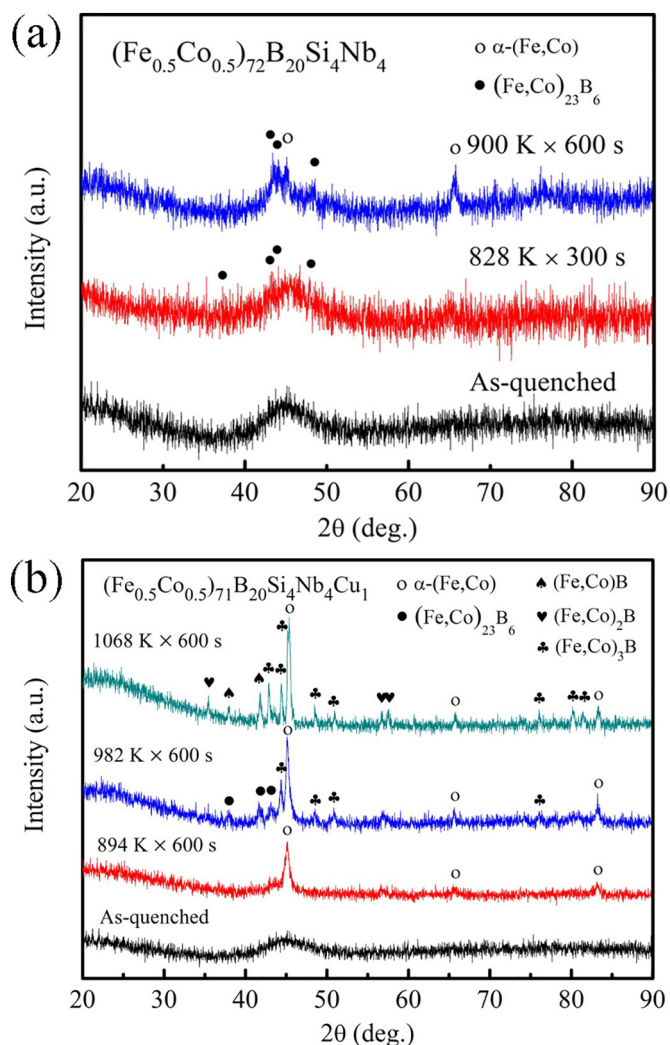


Fig. 2. XRD patterns of (a) $(\text{Fe}_{0.5}\text{Co}_{0.5})_{72}\text{B}_{20}\text{Si}_4\text{Nb}_4$ and (b) $(\text{Fe}_{0.5}\text{Co}_{0.5})_{71}\text{B}_{20}\text{Si}_4\text{Nb}_4\text{Cu}_1$ glassy ribbons annealed at different temperatures and time.

Table 1

The critical diameter (D) and thermal stability data of $(\text{Fe}_{0.5}\text{Co}_{0.5})_{72-x}\text{B}_{20}\text{Si}_4\text{Nb}_4\text{Cu}_x$ ($x = 0, 0.3, 0.4, 0.7$ and 1 at.%) BGAs: glass transition temperature T_g , crystallization temperature T_x , liquidus temperature T_l , undercooled liquid region ΔT_x , and reduced glass transition temperature T_{rg} .

| x | D (mm) | T_g (K) | T_x (K) | T_l (K) | ΔT_x (K) | T_{rg} (T_g/T_l) |
|-----|-------------|--------------|--------------|--------------|---------------------|---------------------------|
| 0 | 3 | 798 ± 3 | 851 ± 4 | 1336 ± 2 | 53 ± 7 | 0.60 ± 0.01 |
| 0.3 | 4 | 806 ± 3 | 862 ± 3 | 1305 ± 2 | 56 ± 6 | 0.62 ± 0.01 |
| 0.4 | 3 | 799 ± 1 | 844 ± 1 | 1328 ± 4 | 45 ± 2 | 0.60 ± 0.01 |
| 0.7 | 3 | 788 ± 2 | 826 ± 6 | 1334 ± 4 | 38 ± 8 | 0.59 ± 0.01 |
| 1 | 3 | 785 ± 5 | 819 ± 2 | 1339 ± 5 | 34 ± 7 | 0.59 ± 0.01 |

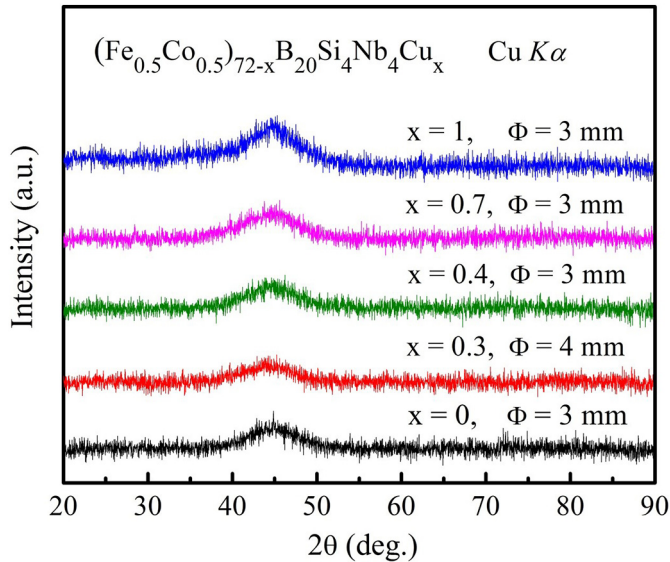


Fig. 3. XRD patterns of $(\text{Fe}_{0.5}\text{Co}_{0.5})_{72-x}\text{B}_{20}\text{Si}_4\text{Nb}_4\text{Cu}_x$ ($x = 0, 0.3, 0.4, 0.7$ and 1 at.%) BGAs with critical diameters.

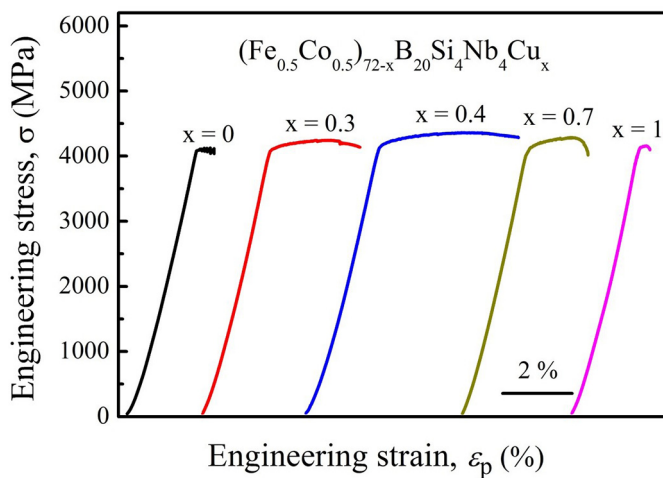


Fig. 4. Compressive engineering stress-strain curves of $(\text{Fe}_{0.5}\text{Co}_{0.5})_{72-x}\text{B}_{20}\text{Si}_4\text{Nb}_4\text{Cu}_x$ ($x = 0, 0.3, 0.4, 0.7$ and 1 at.%) BGAs with diameters of 1 mm.

exothermic peak in the DSC curve, respectively. One can see that the primary precipitation phase is $(\text{Fe,Co})_{23}\text{B}_6$, and the precipitation phases corresponding to the first peak for the FeCoBSiNb glassy alloy without Cu addition are mixed $(\text{Fe,Co})_{23}\text{B}_6$ and $\alpha\text{-(Fe,Co)}$ phases, which is consistent with previous work [7]. However, with 0.3 at.% Cu addition for the FeCoBSiNb glassy alloy in this study, these phases precipitated together through only a single crystallization stage, which means that

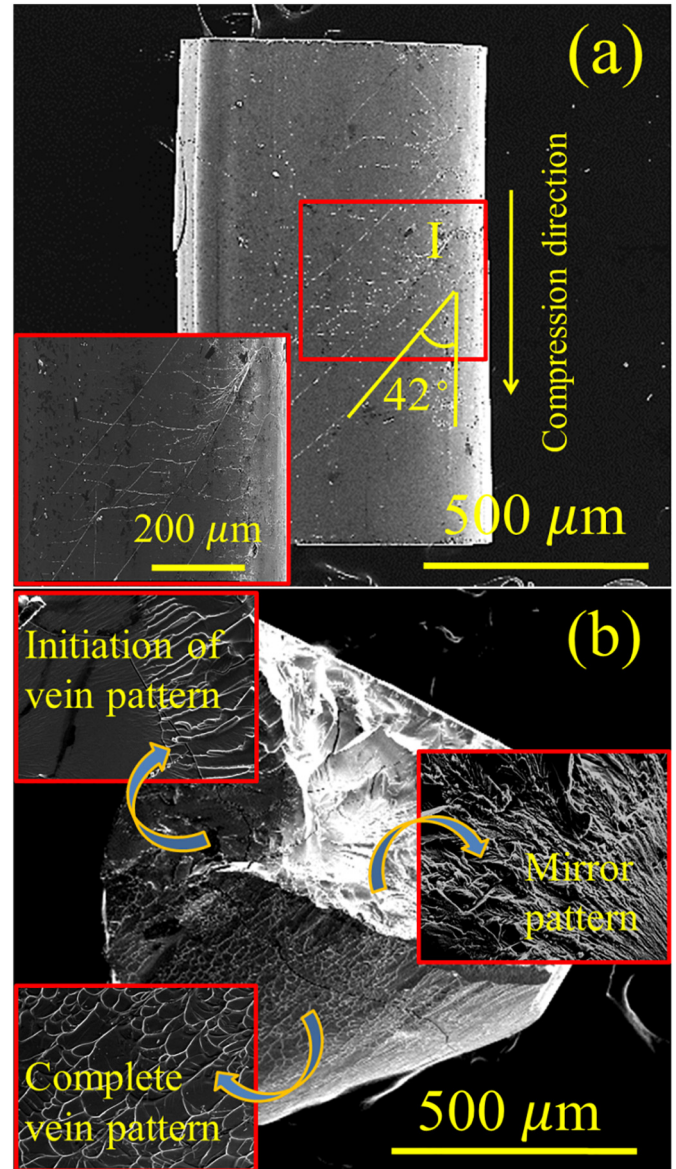


Fig. 5. SEM images of $(\text{Fe}_{0.5}\text{Co}_{0.5})_{71.6}\text{B}_{20}\text{Si}_4\text{Nb}_4\text{Cu}_{0.4}$ BGA: (a) The lateral view of the deformed surface; (b) The images of fragments.

the precipitation of the crystalline phases for the 0.3 at.% Cu-containing glassy alloy is more difficult. Besides, the glass transition temperature (T_g) and crystallization temperature (T_x) shifted to high temperature side as shown in Fig. 1, and the supercooled liquid region ($\Delta T_x = T_x - T_g$) also increased from 53 to 56 K. The liquidus temperature (T_l) value of alloy with 0.3 at.% Cu addition is 1305 K, which is lower than that of other Cu-containing alloys, indicating this alloy is close to the eutectic point, resulting in the largest reduced glass transition temperatures ($T_{rg} = T_g/T_l$) of 0.62 , which is regarded as one of the important parameters for evaluation of glass formation ability. All of the thermal parameters of the Fe-based BGAs are summarized in Table 1. Thus, these results suggest that addition of 0.3 at.% Cu is effective in increasing the thermal stability of the supercooled liquid before crystallization as well as in improving the GFA of alloys. With further increase of Cu content to more than 0.3 at.%, such as for 1 at.% Cu addition, the primary precipitation phase changed to $\alpha\text{-(Fe,Co)}$ phase, which also corresponded to the precipitation phase of the first peak, while the precipitation phases corresponding to the P_2 peak were mixed $(\text{Fe,Co})_{23}\text{B}_6$, $\alpha\text{-(Fe,Co)}$ and $(\text{Fe,Co})_3\text{B}$ phases, and additional $(\text{Fe,Co})\text{B}$ and $(\text{Fe,Co})_2\text{B}$ phases for P_3 peak as shown in Fig. 2 (b), which is in

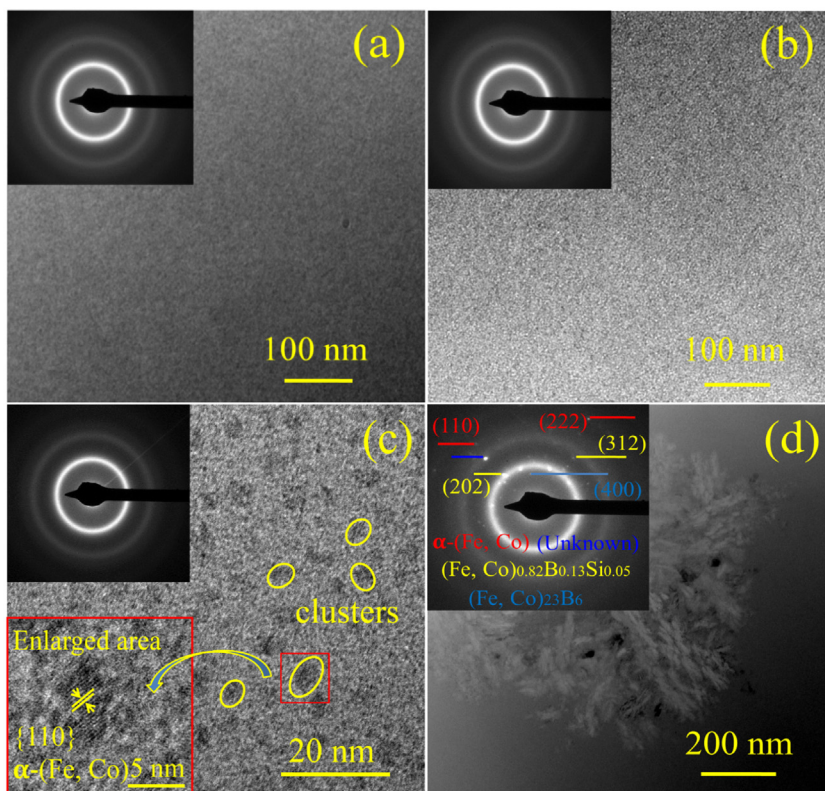


Fig. 6. TEM images and SAED patterns of $(\text{Fe}_{0.5}\text{Co}_{0.5})_{72-x}\text{B}_{20}\text{Si}_4\text{Nb}_4\text{Cu}_x$ BGAs with Cu additions of (a) $x = 0$; (b) $x = 0.3$; (c) $x = 0.4$ and (d) $x = 0.7$, respectively.

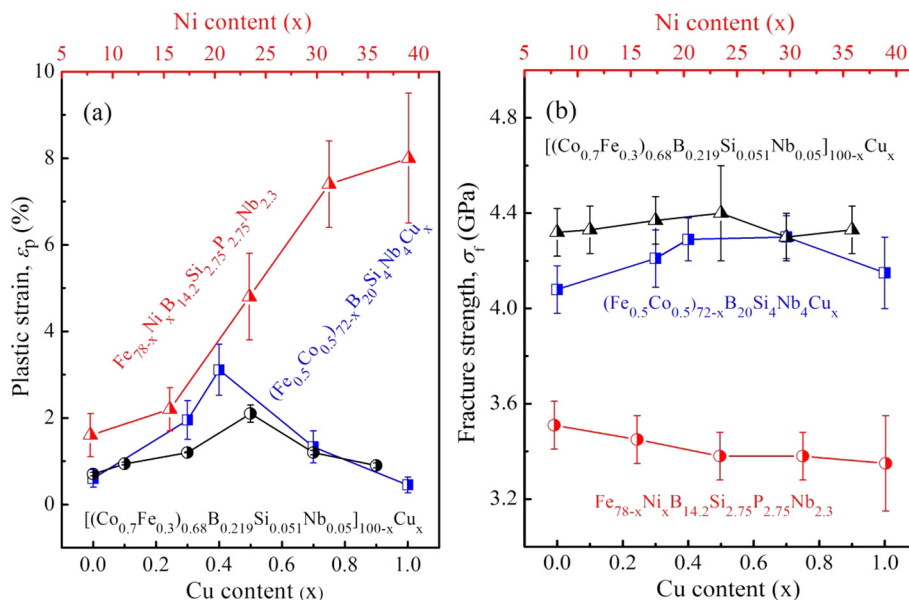


Fig. 7. Compressive plastic strain (a) and fracture strength (b) with Cu/Ni additions for FeCoBSiNb, CoFeBSiNb and FeBSiPNb BGAs.

agreement with previous studies [7,15,16]. As a result, the crystallization behavior was drastically activated through multi-phases transformation. The crystallization behavior of the $(\text{Fe}_{0.5}\text{Co}_{0.5})_{72-x}\text{B}_{20}\text{Si}_4\text{Nb}_4\text{Cu}_x$ ($x = 0, 0.3, 0.4, 0.7$ and 1 at.%) BGAs suggests that proper amount of Cu addition promote the formation of α -(Fe,Co) phase in the glassy matrix, which is expected to affect the mechanical and soft magnetic performance of the alloys.

Based on the above analysis, the proper Cu addition plays an important role during crystallization process. The Cu-free glassy alloy is a chemically uniform amorphous solid solution and its primary

precipitation phase is $(\text{Fe,Co})_{23}\text{B}_6$. With minor Cu addition, as Cu has a large positive heat of mixing with Fe/Co [17], Fe/Co atoms are rejected from Cu clusters and would pileup at the Cu/amorphous interface [18]. Then the heterogeneous nucleation at the Cu/amorphous interface is chemically more favorable than the homogeneous nucleation from the amorphous phase. Meanwhile, the fcc-Cu (111) and bcc α -(Fe,Co) (110) have very good matching [18]. Thus, α -(Fe,Co) will nucleate on the fcc-Cu (111) surface which can provide a low interfacial energy. In addition, the Fe_{23}B_6 phase has a complex face-centered cubic structure with a large lattice parameter of 96 atoms and its precipitation from the

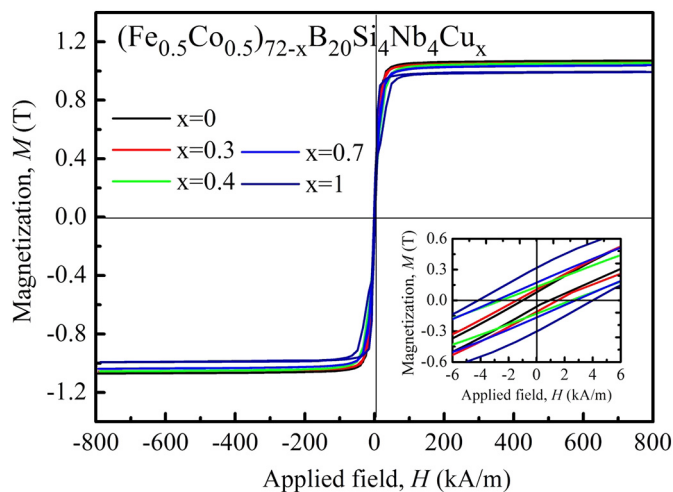


Fig. 8. DC hysteresis loops of $(\text{Fe}_{0.5}\text{Co}_{0.5})_{72-x}\text{B}_{20}\text{Si}_4\text{Nb}_4\text{Cu}_x$ ($x = 0, 0.3, 0.4, 0.7$ and 1 at.%) glassy ribbons. The inset is the magnification of partial hysteresis curve at the vicinity of $H = 0$.

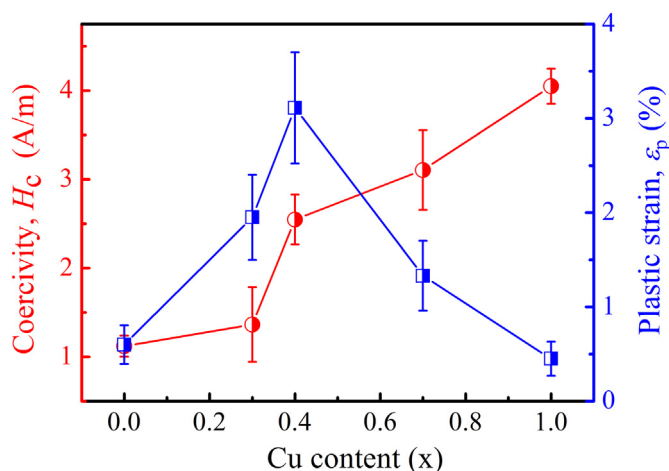


Fig. 9. The coercivity and plastic strains of $(\text{Fe}_{0.5}\text{Co}_{0.5})_{72-x}\text{B}_{20}\text{Si}_4\text{Nb}_4\text{Cu}_x$ ($x = 0, 0.3, 0.4, 0.7$ and 1 at.%) glassy alloys.

network-like glassy structure requires high energy and long-range atomic rearrangements of constituent elements [19]. Thus, the competitive formation of the Fe_{23}B_6 and $\alpha\text{-(Fe,Co)}$ (110) results in a single crystallization stage on DSC curve for 0.3 at.% Cu-containing glassy alloy, which promotes a high thermal stability and large GFA. However, with more Cu addition, T_g gradually decreases, indicating the reducing of thermal stability of glass alloys. Considering this, we tried to prepare cylindrical glassy alloy rods with different diameters. Fig. 3 shows XRD patterns of the cast alloy rods. Only broad peaks without any crystallization are observed for all of the bulk samples, indicating the formation of a glassy phase in the diameter range up to 4 mm. Thus, the BGAs with a single glassy phase are developed in the Cu content of $x = 0\text{--}1$ and the largest diameter is 4 mm with the composition of $x = 0.3$. The mechanical properties of the $(\text{Fe}_{0.5}\text{Co}_{0.5})_{72-x}\text{B}_{20}\text{Si}_4\text{Nb}_4\text{Cu}_x$ ($x = 0, 0.3, 0.4, 0.7$ and 1 at.%) glassy rods with a diameter of 1 mm were measured by compressive tests. The stress-strain curves for all samples are linear up to the elastic strain of 2%, with distinct plastic deformation after yielding, as shown in Fig. 4. The $(\text{Fe}_{0.5}\text{Co}_{0.5})_{72-x}\text{B}_{20}\text{Si}_4\text{Nb}_4\text{Cu}_x$ alloy system exhibits high fracture strength (σ_f) of 4080–4310 MPa. The observed strain-hardening behavior is consistent with the deformation behavior of other Fe-based amorphous alloys reported before, which was usually attributed to the continuous initiation of multiple shear bands with different critical shear stress in

different regions of the specimen [20,21]. The strain-hardening exponent, n , has been calculated for FeCoBSiNb alloys with Cu addition using the equation: $\sigma = K\epsilon^n$, where σ and ϵ are the true-stress and true-strain, respectively, and K is the strength coefficient [22]. It was found that FeCoBSiNb alloy with 0.7 at.% Cu addition showed the higher n of 0.233 ± 0.019 than that of other alloys (0.011 ± 0.003 , 0.111 ± 0.004 , 0.103 ± 0.002 , and 0.041 ± 0.005 for alloys with 0, 0.3, 0.4 and 1.0 at.% Cu addition, respectively), indicating the better uniform deformation ability for former alloy. Moreover, the plastic strain (ϵ_p) firstly increases and then decreases with the increment of Cu content. Especially, with Cu content increasing to 0.3 and 0.4 at.%, the plastic strain increases up to 2.4% and 3.7%, respectively, revealing that $(\text{Fe}_{0.5}\text{Co}_{0.5})_{71.6}\text{B}_{20}\text{Si}_4\text{Nb}_4\text{Cu}_{0.4}$ BGA simultaneously possesses both large plasticity and high compressive strength.

The morphology of the deformation and fracture surfaces after compression tests were analyzed to reveal the mechanism of the mechanical behaviors of the Cu added FeCoBSiNb BGAs. Fig. 5 shows SEM images of the side surface of $(\text{Fe}_{0.5}\text{Co}_{0.5})_{71.6}\text{B}_{20}\text{Si}_4\text{Nb}_4\text{Cu}_{0.4}$ specimen after compression loading prior to failure. The localized main shear band propagates in a shear angle of 42° to the compressive axis [see Fig. 5 (a)]. As shown in the inset of Fig. 5 (a), a great number of secondary shear bands parallel to the main shear band, as well as multiple shear bands are observed on the surface of the rod. These shear bands are deflected and bifurcated several times, indicating that the propagation of main shear band encounters many obstacles and also induces a large number of shear bands formation, branching and intersection with each other, which can effectively suppress the development of shear band during compressive loading. Therefore, it is not easy for the main shear band to transform into cracks and the plastic deformation ability of the Cu-containing Fe-based BGA is enhanced. The fracture surfaces of $(\text{Fe}_{0.5}\text{Co}_{0.5})_{71.6}\text{B}_{20}\text{Si}_4\text{Nb}_4\text{Cu}_{0.4}$ BGA were also examined as shown in Fig. 5 (b). The surface contains not only mirror-like structures from brittle failure, but also vein-like patterns that are the characteristics of ductile fracture behavior, indicating the improved plasticity in some regions. The enlarged images of the initial and complete vein patterns are shown in the insets, which reveal details of the melted liquid flow on the fracture surface as the vein pattern structure is normally regarded as the solidification form of melted liquid flow. This phenomenon indicates the occurrence of melting behavior caused by remarkable temperature rise due to the high elastic energy released during compression [23], which is similar to the molten droplets that we previously reported [24]. It is worthy to note that these findings are different from the brittle fracture mechanism of similar components reported before [25]. Thus, the appearance of the abundant-multiple shear bands together with well-developed vein patterns, which are the characteristic of metallic glasses with good ductility [26,27], can evidently verify the enhanced plasticity of $(\text{Fe}_{0.5}\text{Co}_{0.5})_{71.6}\text{B}_{20}\text{Si}_4\text{Nb}_4\text{Cu}_{0.4}$ BGA.

To further explore the underlying mechanism of the large plasticity for $(\text{Fe}_{0.5}\text{Co}_{0.5})_{71.6}\text{B}_{20}\text{Si}_4\text{Nb}_4\text{Cu}_{0.4}$ BGA, the microstructures of the as-cast $(\text{Fe}_{0.5}\text{Co}_{0.5})_{72-x}\text{B}_{20}\text{Si}_4\text{Nb}_4\text{Cu}_x$ ($x = 0, 0.3, 0.4$ and 0.7 at.%) glassy rods were investigated by TEM as shown in Fig. 6. From Figs. 6 (a) and (b), the uniform structures are identified by TEM images for the samples with Cu addition of 0 and 0.3 at.%, and the SAED patterns only consisting of a single diffraction halo without sharp diffraction rings reveal their typical glassy structures. However, in Fig. 6 (c), although the SAED pattern still illustrates an obvious glassy feature with a diffused diffraction halo, the nano-scale inhomogeneous structures of short-range order clusters with a diameter of 2–4 nm can be found. The lattice fringes as indicated by yellow bars in the inset of Fig. 6 (c) correspond to the (110) plane of bcc $\alpha\text{-(Fe,Co)}$ phase. Previous reports reveal that the precipitation of the second phases from the glassy matrix not only change the free volume distribution of BGAs and ultimately promote the nucleation of multiple shear bands throughout the overall material [28], but also play an important role in hindering the propagation of shear bands [29–31], enabling shear bands blocked or branched with

each other, leading to the large plasticity. Therefore, for the $(\text{Fe}_{0.5}\text{Co}_{0.5})_{71.6}\text{B}_{20}\text{Si}_4\text{Nb}_4\text{Cu}_{0.4}$ alloy with heterogeneous structure of α -(Fe,Co) phases, the nanoparticles may act as the initiation sites for the multiple shear bands in the glassy matrix under compression to activate the homogeneous and abundant-multiple shear bands, as well as the hindering sites for the shear bands to deflect their direction during their propagation under loading. As a result, the alloy with heterogeneous structures could effectively hinder the sudden instability of the shear bands and form a great number of branching shear bands, resulting in a distinct enhancement on the room temperature plasticity. However, as Cu content increases to 0.7 at.% for $(\text{Fe}_{0.5}\text{Co}_{0.5})_{72-x}\text{B}_{20}\text{Si}_4\text{Nb}_4\text{Cu}_x$ BGA, the nanoparticles with size more than 200 nm can be seen, as shown in Fig. 6 (d). In addition, it is confirmed from the SAED patterns that this sample contains multiple crystal phases precipitated from the glassy matrix, including α -(Fe,Co), $(\text{Fe,Co})_{23}\text{B}_6$, $(\text{Fe,Co})_{0.82}\text{B}_{0.13}\text{Si}_{0.05}$ and some unknown phases. Generally, the brittle Fe–B microcrystalline phase (e.g. Fe_{23}B_6 -type phase) in the glassy matrix will cause the embrittlement of the BGA composites [12,32]. In this Fe-based system, the brittle $(\text{Fe,Co})_{23}\text{B}_6$ phases and grain coarsening in the $(\text{Fe}_{0.5}\text{Co}_{0.5})_{71.3}\text{B}_{20}\text{Si}_4\text{Nb}_4\text{Cu}_{0.7}$ BGA might be the main reason for its decreased plasticity. In conclusion, the α -(Fe,Co) phases with an appropriate size resulting from the optimum Cu addition are considered as an important factor for improving the plasticity of Fe-based BGAs.

The compressive plastic strain and fracture strength for FeCoBSiNb, CoFeBSiNb [10] and FeBSiPnB [11] BGAs with Cu/Ni addition are compared in Fig. 7. It can be clearly seen that both the plastic strain and fracture strength of the FeCoBSiNbCu BGA investigated in this work are between those of the CoFeBSiNbCu and FeNiBSiPnB BGAs. The plastic strain of FeCoBSiNb BGAs with minor Cu addition is obviously increased compared to that of CoFeBSiNb BGAs with Cu addition [Fig. 7 (a)]; while the fracture strength of the FeCoBSiNbCu maintains at a higher level compared to that of FeBSiPnB BGAs with Ni addition [Fig. 7 (b)]. In summary, a new FeCoBSiNbCu BGA with large fracture strength and high plastic strain has been obtained with minor Cu addition.

In addition to the high GFA and excellent mechanical properties, the $(\text{Fe}_{0.5}\text{Co}_{0.5})_{72-x}\text{B}_{20}\text{Si}_4\text{Nb}_4\text{Cu}_x$ glassy alloys exhibit good soft-magnetic properties as well. Fig. 8 shows the hysteresis loops of the $(\text{Fe}_{0.5}\text{Co}_{0.5})_{72-x}\text{B}_{20}\text{Si}_4\text{Nb}_4\text{Cu}_x$ glassy alloys. One can see that the B_s values of Cu-containing glassy alloys are within the range of 0.99–1.07 T, although they decrease slightly with increasing Cu alloying content due to the dilution of ferromagnetic constituents [33]. The variations of H_c for melt-spun $(\text{Fe}_{0.5}\text{Co}_{0.5})_{72-x}\text{B}_{20}\text{Si}_4\text{Nb}_4\text{Cu}_x$ glassy alloys are also obtained as shown in Fig. 9. The H_c increases slightly from 1.1 to 1.4 A/m with the Cu addition from 0 to 0.3 at.%, and then increases up to 4.0 A/m with further Cu addition. According to the random anisotropy model [34], the H_c varies with the grain size (D) as $H_c \propto D^6$. The small H_c of $(\text{Fe}_{0.5}\text{Co}_{0.5})_{72-x}\text{B}_{20}\text{Si}_4\text{Nb}_4\text{Cu}_x$ ($x = 0$ and 0.3) can be attributed to the homogeneous amorphous structures. As the Cu addition increases from 0.3 to 1 at.%, the grain size of the nanocrystalline phases enlarges from 2 to 200 nm. Moreover, the precipitations of the hard magnetic phases (Fe,Co)-boride compounds have been found in the alloys with more than 0.3 at.% Cu content. Both the formation of (Fe,Co)-borides and grain coarsening degrade the soft magnetic properties, leading to the increase of H_c . This is almost consistent with the trend of the plastic strain with Cu content, as shown by the blue line in Fig. 9. As a result, the excellent mechanical properties and satisfying soft magnetic performance were obtained for the FeCoBSiNb alloy with 0.4 at.% Cu addition, which exhibits the high σ_f over 4000 MPa, large ϵ_p of 3.7%, high B_s of 1.05 T and low H_c of 2.5 A/m.

4. Conclusions

A minor Cu addition of 0.3 at.% was found to be effective in improving the thermal stability of the glassy structure, and 0.4 at.% Cu addition was found to be effective for improving the plasticity of the

$(\text{Fe}_{0.5}\text{Co}_{0.5})_{72-x}\text{B}_{20}\text{Si}_4\text{Nb}_4\text{Cu}_x$ glassy alloy system. The 0.3 at.% Cu-containing BGA with a diameter of 4 mm was successfully prepared. The 0.4 at.% Cu-containing BGA exhibits high σ_f over 4000 MPa, large ϵ_p of 3.7%, combined with high B_s of 1.05 T and low H_c of 2.5 A/m. This work reveals that the mechanical and soft magnetic properties are sensitive to the heterogeneity of alloy introduced by minor Cu addition. By micro-alloying Cu element, although the B_s is reduced, the formation of nano-scale α -(Fe,Co) phases from amorphous matrix enhances the room temperature plasticity by hindering the propagation of shear bands and promoting multiple shearing. This study has a guiding significance for deeply understanding the poor plasticity of Fe-based BGA and also provides a guidance to design high performance Fe-based BGAs with large glass-forming ability, good mechanical and soft magnetic properties for the future engineering applications.

Acknowledgments

This work was supported by the National Natural Science Foundation of China (Grant Nos. 51631003, 51501037 and 51871237), and the Jiangsu key laboratory for advanced metallic materials (Grant No. BM2007204).

References

- [1] A. Inoue, Y. Shinohara, J.S. Gook, Thermal and magnetic properties of bulk Fe-based glassy alloys prepared by copper mold casting, *Mater. Trans.* 36 (1995) 1427–1433.
- [2] T.D. Shen, R.B. Schwarz, Bulk ferromagnetic glasses prepared by flux melting and water quenching, *Appl. Phys. Lett.* 75 (1999) 49–51.
- [3] A. Inoue, B.L. Shen, Soft magnetic bulk glassy Fe–B–Si–Nb alloys with high saturation magnetization above 1.5 T, *Mater. Trans.* 43 (2002) 766–769.
- [4] B.L. Shen, A. Inoue, Bulk glassy Fe–Ga–P–C–B–Si alloys with high glass-forming ability, high saturation magnetization and good soft magnetic properties, *Mater. Trans.* 49 (2002) 1235–1239.
- [5] Z.P. Lu, C.T. Liu, J.R. Thompson, W.D. Porter, Structural amorphous steels, *Phys. Rev. Lett.* 92 (2004) 245503.
- [6] A. Inoue, B.L. Shen, C.T. Chang, Super-high strength of over 4000 MPa for Fe-based bulk glassy alloys in $[(\text{Fe}_{1-x}\text{Co}_x)_{0.75}\text{B}_{0.2}\text{Si}_{0.05}]_{96}\text{Nb}_4$ system, *Acta Mater.* 52 (2004) 4093–4099.
- [7] A. Inoue, B.L. Shen, A new Fe-based bulk glassy alloy with outstanding mechanical properties, *Adv. Mater.* 36 (2005) 2189–2192.
- [8] B.L. Shen, A. Inoue, C.T. Chang, Superhigh strength and good soft-magnetic properties of (Fe,Co)-B–Si–Nb bulk glassy alloys with high glass-forming ability, *Appl. Phys. Lett.* 85 (2004) 4911–4913.
- [9] B.L. Shen, M. Akiba, A. Inoue, Excellent soft-ferromagnetic bulk glassy alloys with high saturation magnetization, *Appl. Phys. Lett.* 88 (2006) 131907.
- [10] G.L. Zhang, Q.Q. Wang, C.C. Yuan, W.M. Yang, J. Zhou, L. Xue, F. Hu, B.A. Sun, B.L. Shen, Effects of Cu additions on mechanical and soft-magnetic properties of CoFeBSiNb bulk metallic glasses, *J. Alloys Compd.* 737 (2018) 815–820.
- [11] J. Zhou, W.M. Yang, C.C. Yuan, B.A. Sun, B.L. Shen, Ductile FeNi-based bulk metallic glasses with high strength and excellent soft magnetic properties, *J. Alloys Compd.* 742 (2018) 318–324.
- [12] B.L. Shen, H. Men, A. Inoue, Fe-based bulk glassy alloy composite containing in situ formed α -(Fe,Co) and $(\text{Fe,Co})_{23}\text{B}_6$ microcrystalline grains, *Appl. Phys. Lett.* 89 (2006) 101915.
- [13] K. Hono, D.H. Ping, M. Ohnuma, H. Onodera, Cu clustering and Si partitioning in the early crystallization stage of an $\text{Fe}_{73.5}\text{Si}_{13.5}\text{B}_9\text{Nb}_3\text{Cu}_1$ amorphous alloy, *Acta Mater.* 47 (1999) 997–1006.
- [14] Y.M. Chen, T. Ohkubo, M. Ohta, Y. Yoshizawa, K. Hono, Three-dimensional atom probe study of Fe–B-based nanocrystalline soft magnetic materials, *Acta Mater.* 57 (2009) 4463–4472.
- [15] W.M. Yang, H.S. Liu, X.D. Fan, L. Xue, C.C. Dun, B.L. Shen, Enhanced glass forming ability of Fe-based amorphous alloys with minor Cu addition, *J. Non-Cryst. Solids* 419 (2015) 65–68.
- [16] M. Stoica, P. Ramasamy, I. Kaban, S. Scudino, M. Nicoara, G. Vaughan, J. Wright, R. Kumar, J. Eckert, Structure evolution of soft magnetic $(\text{Fe}_{36}\text{Co}_{36}\text{B}_{19.2}\text{Si}_{4.8}\text{Nb}_4)_{100-x}\text{Cu}_x$ ($x = 0$ and 0.5) bulk glassy alloys, *Acta Mater.* 95 (2015) 335–342.
- [17] A. Takeuchi, A. Inoue, Classification of bulk metallic glasses by atomic size difference, heat of mixing and period of constituent elements and its application to characterization of the main alloying element, *Mater. Trans.* 46 (2005) 2817–2829.
- [18] K. Hono, D.H. Ping, M. Ohnuma, H. Onodera, Cu clustering and Si partitioning in the early crystallization stage of an $\text{Fe}_{73.5}\text{Si}_{13.5}\text{B}_9\text{Nb}_3\text{Cu}_1$ amorphous alloy, *Acta Mater.* 47 (1999) 997–1006.
- [19] J.H. Zhang, B.L. Shen, Z.D. Zhang, Crystallization behaviors of FeSiBPMo bulk metallic glasses, *J. Non-Cryst. Solids* 360 (2013) 31–35.
- [20] K.F. Yao, C.Q. Zhang, Fe-based bulk metallic glass with high plasticity, *Appl. Phys. Lett.* 90 (2007) 061901.
- [21] J.M. Park, G. Wang, R. Li, N. Mattern, J. Eckert, D.H. Kim, Enhancement of plastic

- deformability in Fe-Ni-Nb-B bulk glassy alloys by controlling the Ni-to-Fe concentration ratio, *Appl. Phys. Lett.* 96 (2010) 031905.
- [22] M.D. Demetriou, M.E. Launey, G. Garrett, J.P. Schramm, D.C. Hofmann, W.L. Johnson, R.O. Ritchie, A damage-tolerant glass, *Nat. Mater.* 10 (2011) 123–128.
- [23] J.J. Lewandowski, A.L. Greer, Temperature rise at shear bands in metallic glasses, *Nat. Mater.* 5 (2006) 15–18.
- [24] B.L. Shen, C.T. Chang, A. Inoue, Formation, ductile deformation behavior and soft-magnetic properties of (Fe,Co,Ni)-B-Si-Nb bulk glassy alloys, *Intermetallics* 15 (2007) 9–16.
- [25] M. Stoica, S. Scudino, J. Bednarčík, I. Kaban, J. Eckert, FeCoSiBNbCu bulk metallic glass with large compressive deformability studied by time-resolved synchrotron X-ray diffraction, *J. Appl. Phys.* 115 (2014) 152–161.
- [26] S.F. Guo, N. Li, C. Zhang, L. Liu, Enhancement of plasticity of Fe-based bulk metallic glass by Ni substitution for Fe, *J. Alloys Compd.* 504 (2010) S78–S81.
- [27] J.F. Wang, W.B. Cao, L.G. Wang, S.J. Zhu, S.K. Guan, L. Huang, R. Li, T. Zhang, Fe-Al-P-C-B bulk metallic glass with good mechanical and soft magnetic properties, *J. Alloys Compd.* 637 (2015) 5–9.
- [28] A. Makino, X. Li, K. Yubuta, C.T. Chang, T. Kubota, A. Inoue, The effect of Cu on the plasticity of Fe-Si-B-P-based bulk metallic glass, *Scr. Mater.* 60 (2009) 277–280.
- [29] X. Li, H. Kato, K. Yubuta, A. Makino, A. Inoue, Improved plasticity of iron-based high-strength bulk metallic glasses by copper-induced nanocrystallization, *J. Non-Cryst. Solids* 357 (2011) 3002–3005.
- [30] J.M. Parka, D.H. Kimb, J. Eckerta, Enhanced plasticity of Fe-Nb-B-(Ni,Cu) bulk metallic glasses by controlling the heterogeneity and elastic constants, *J. Alloys Compd.* 536 (2012) S70–S73.
- [31] C.L. Zhao, C.C. Dun, Q.K. Man, B.L. Shen, Enhancement of plastic deformation in FeCoNbB bulk metallic glass with superhigh strength, *Intermetallics* 32 (2013) 408–412.
- [32] S.F. Guo, L. Liu, N. Li, Y. Li, Fe-based bulk metallic glass matrix composite with large plasticity, *Scr. Mater.* 62 (2010) 329–332.
- [33] M. Aykol, M.V. Akdeniz, A.O. Mekhrabov, Solidification behavior, glass forming ability and thermal characteristics of soft magnetic Fe-Co-B-Si-Nb-Cu bulk amorphous alloys, *Intermetallics* 19 (2011) 1330–1337.
- [34] G. Herzer, Grain size dependence of coercivity and permeability in nanocrystalline ferromagnets, *IEEE Trans. Magn.* 26 (1990) 1397–1402.